SIMULATION OF THE MECHANICAL BEHAVIOR OF ADHESIVELY BONDED JOINTS BY USING MESHLESS COHESIVE SEGMENTS AND SSPH BASIS FUNCTIONS

C. L. Tsai, Y. L. Guan, D. C. Ohanehi, J. G. Dillard, D. A. Dillard, R. C. Batra
Department of Engineering Science and Mechanics, MC0219
223 Norris Hall, Blacksburg, VA 24061
cltsai@vt.edu

1. Abstract

Adhesives have become the method of choice for many structural joining applications. Thus there is need for improved understanding of adhesive joint performance under a variety of loading conditions. Various numerical methods have been proposed to predict the failure behavior of adhesive bonded material systems. In these methods, a cohesive zone model (CZM) is widely used to analyze the crack initiation and failure loci in adhesively bonded joints. The CZM incorporates a traction-separation law which relates the cohesive stress with the displacement jump between abutting particles of the cohesive segment. Whereas the fracture energy is derived from experimental data, the initial stiffness and critical cohesive stress in the CZM are obtained through the comparison of results of numerical simulations with the experimental data. We have used the central composite design technique to find optimal values of the CZM parameters by assuming a second order mathematical model.

A numerical approach to simulate crack initiation and propagation has been developed by implementing cohesive zone segments in the meshless method using the symmetric smoothed particle hydrodynamics (SSPH) basis functions. Unlike in the finite element method (FEM) where a crack generally follows the path between element boundaries, in the meshless method a crack can follow the path dictated by the physics of the problem. This numerical technique has been used to study the initiation and propagation of a crack in a double cantilever beam (DCB) specimen under mode I loading. The computed results are found to agree well with experimental findings.

2. Introduction

Fracture behavior in adhesively bonded material systems subjected to single mode or mixed mode loading is of significant interest in a number of industries including those engaged in biomedical implants, construction, microelectronics, mining, transportation, and energy. In classical fracture mechanics, a singular stress field around the crack tip, the stress intensity factor and the T-stress are used to simulate the crack path and the failure process. The CZM [1-2] was proposed to simulate the crack initiation and propagation. The CZM is based on the consideration that infinite stresses predicted in classical fracture mechanics are not realistic. The CZM describes material separation with a traction-separation law and it can be applied to continuum deformation fields. The CZM is widely used in conjunction with the FEM to simulate the fracture behavior in a variety of materials, e.g. cracks in brittle metals, debonding in adhesives and delamination in composite materials [3-4]. Different forms of the traction-separation law have been developed, but they all have similar characteristic. As the cohesive surfaces start to separate, the traction increases until a maximum value is reached, and subsequently the traction decreases with an increase in the separation and equals zero at complete separation. It avoids stress singularities, and the tractions depend on the relative displacements between the two surfaces.

In a meshless method, a structured distribution of particles or nodes is not necessary, and one can simulate crack propagation along the path dictated by the physics of the problem. The meshless method combined with the CZM was first developed to simulate the Mode I failure and quasi-static delamination by using the moving least squares (MLS) basis functions.

In this work, boundary value problems closely simulating test conditions have been numerically analyzed by using the in-house developed software based on the meshless local Petrov-Garlekin formulation of the problem. The trial solution is expressed as a linear combination of SSPH basis functions [5]. Optimum values of CZM parameters have been found through a systematic procedure that compares numerically computed load-displacement curves of DCB specimens under mode I loading with the corresponding test data for one case. Subsequently, these values are used to compute results for other configurations and computed results are compared with experimental findings.

3. Validation of mathematical model

The meshless method with cohesive segments is used to analyze deformations of the DCB specimen tested experimentally, and computed results are compared with the experimental data and also with numerical results available in the literature that were obtained by using the FEM. A schematic sketch of the problem studied is shown in Fig. 1 where the specimen length $L = 120\ mm$, the adherend thickness $= 15\ mm$,

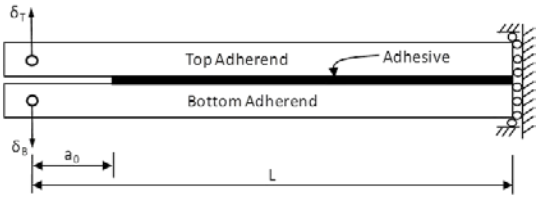

Figure 1. Schematic sketch of the DCB problem studied.

the adhesive thickness $= 0.3\ mm$, and the pre-notched crack length $a_0 = 40\ mm$. Values of material parameters of each adherend are Young's modulus $E = 70\ GPa$, and Poisson's ratio $\upsilon = 0.3$. For the adhesive: $E = 880\ MPa$ and $\upsilon = 0.15$. The CZM parameters are: fracture toughness $\Gamma_I = 500\ N/m$ and critical cohesive stress $\tau_{cr} = 4.0\ MPa$.

The adherends and the adhesive in the DCB specimen are assumed to deform in a state of plane strain. The traction-separation law is exhibited in Figure 2 with values of the CZM parameters the same as those used in [7]. In Figure 3, the presently computed load-displacement curve is compared with that obtained experimentally by Pirondi et al. [6] and also with that computed by Alfano et al. [7] using the FEM. The differences in the experimentally found peak load and that numerically computed using the FEM and the SSPH method equal 6.7% and 3.1%, respectively.

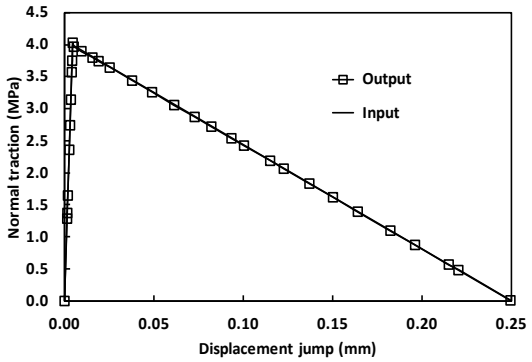

Figure 2. Traction separation law for pure mode I

4. Mechanical behavior of DCB specimen

The boundary-value problems for the DCB specimens tested experimentally have been numerically analyzed. Values of various material and geometric parameters are as follows. Adherend: $E = 70\ GPa$ and $\upsilon = 0.3$; adhesive: $E = 3\ GPa$, $\upsilon = 0.33$ and $\Gamma_I = 488\ N/m$; length (L) of DCB specimen $= 240\ mm$, adherend thickness $= 12.7\ mm$, adhesive thickness $= 0.30\ mm$; the initial crack length $a_0 = 40\ mm$. As was done in experiments, the specimen is deformed by prescribing the axial displacements, δ_T and δ_B, for the top and the bottom adherends, respectively. A plane strain state of deformation is assumed to prevail in the DCB specimen.

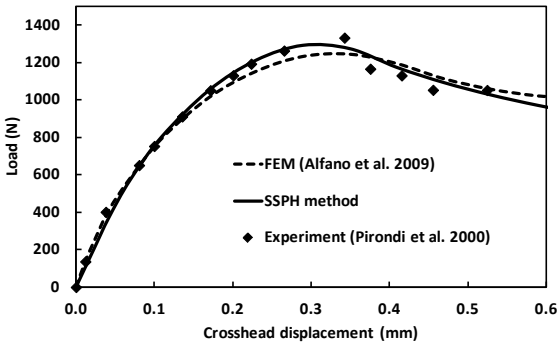

Figure 3. Comparison of the numerically computed and experimentally observed load vs. displacement curves.

With the fracture toughness determined from the experimental data, the traction-separation law depicted in Fig. 2 can be fully constructed with two parameters: the critical cohesive stress and the initial stiffness. The central composite design technique [8] was used to find optimal values of these parameters by assuming a second order mathematical model

$$y = \beta_0 + \sum_{i=1}^{k} \beta_i x_i + \sum_{i=1}^{k} \beta_{ii} x_i^2 + \sum_{i=1}^{k} \beta_{ij} x_i x_j, \ k = 2,$$

where coefficients β_0, β_i, β_{ii} and β_{ij} are to be determined, x_i is the design variable and y is the objective function defined as

$$y = \lambda \left(\sqrt{\sum_{i=1}^{n} (f_{\exp}^{i} - f_{num}^{i})^2} \Big/ \sqrt{\sum_{i=1}^{n} (f_{\exp}^{i})^2} \right) + (1-\lambda) \left| \frac{P_{\exp} - P_{num}}{P_{\exp}} \right|$$

The objective function, y, is composed of two parts; the difference in the experimental and the computed values of loads for a given displacement and the difference in the peak values of the experimental and the computed loads. The number, n, of sampling points is taken as 100 and λ is a scalar number between 0 and 1. We suggest that one should take λ = 0.5. The response surface of the objective function for various values of the critical cohesive stress and the initial interface stiffness, shown in Figure 4, has the minimum value when $\tau_{cr} = 11.6\ MPa$, $K_0 = 2940\ MPa/mm$.

The load-displacement curve computed with the in-house developed software is compared in Figure 5 with the experimental ones for five specimens. The difference between the computed and the measured peak loads is found to be less than 7.0%. Figure 6 shows a comparison of the computed load vs. the crack

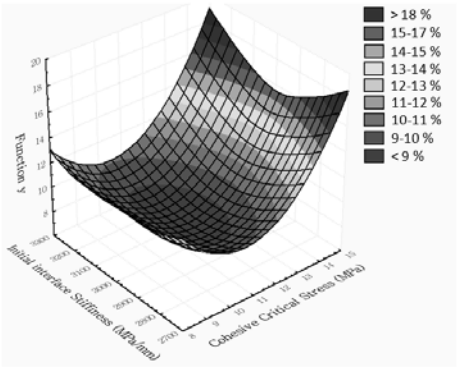

Figure 4. Plot of function *y* against the critical cohesive stress and the initial stiffness.

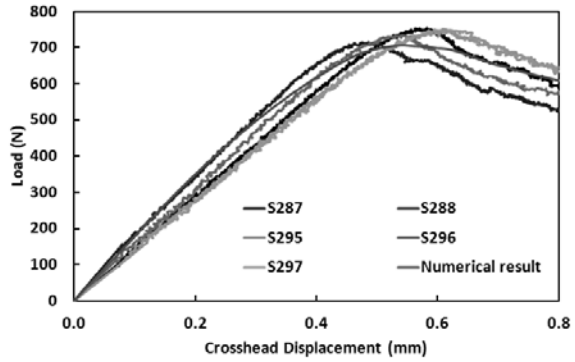

Figure 5. Comparison of the computed and experimental (5 specimens) load-displacement curves.

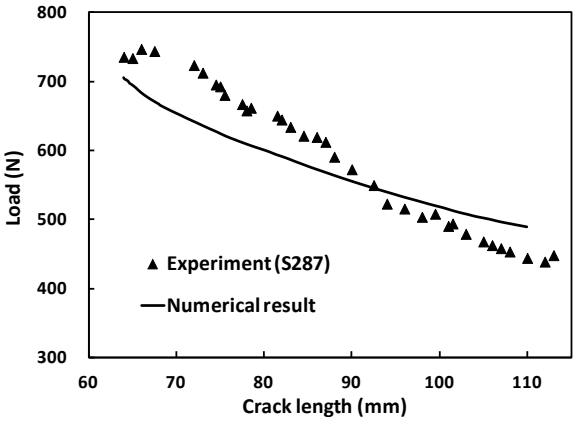

Figure 6. Comparison of the computed and the experimental load vs. crack length curve.

length from the SSPH basis functions with the experimental one. The computed J-integral, i.e., the strain energy release rate, for specimen S287 is compared in Figure 7 with the strain energy release rate determined from the experimental data. The computed fracture energy is 13% less than that found from the test data.

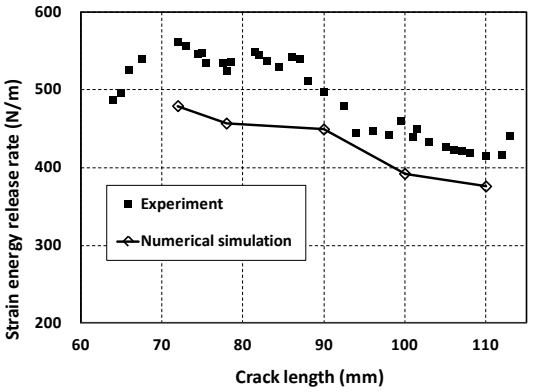

Figure 7. Comparison of the computed and the experimental strain energy release rate vs. the crack length for specimen S287.

5. Conclusions

The CZM has been implemented in a meshless method using the SSPH basis functions, and the software has been used to analyze the mechanical deformations of adhesively bonded joints. The CZM parameters have been determined through a systematic procedure. The computed load-displacement curves for DCB specimens deformed in mode I have been found to agree well with the corresponding test findings. The difference between the computed and the experimental peak loads is less than 7%, and that between the cross-head displacements at the peak load is less than 13%.

6. Acknowledgements

This work was supported by the National Science Foundation grant (NSF/CMMI Award No. 0826143) to Virginia Polytechnic Institute and State University.

7. References

1. D.S. Dugdale, J. Mechanics and Physics of Solids, 1960, 8, pp100-104.
2. G. Barenblatt, Advanced in Applied Mechanics, 1962, 7, pp55-129.
3. A. Hattiangadi and T. Siegmund, J. Mechanics and Physics of Solids, 2004, 52, pp533-566.
4. K. Park, G.H. Paulino and J.R. Roesler, Engineering Fracture Mechanics, 2008, 75, pp3806-3818.
5. R.C. Batra and G.M. Zhang, Computational Mechanics, 2008, 41, pp527-545.
6. A. Pirondi and G. Nicoletto, Proceedings of the 15th National Congress of the Italian Group of Fracture, 2000, pp459-466.
7. M. Alfano M, F. Furgiuele, A. Leonardi, C. Maletta, G.H. Paulino, International J. of Fracture, 2009, 157, pp193-204.
8. J. Sack, W.J. Welch, T.J. Mitchell, J. of the Royal Society Statistical Science, 1989, 4, pp409-435.